Electronic Supplementary Material (ESI) for RSC Advances.
This journal is © The Royal Society of Chemistry 2017

Electronic Supplementrary Information

for the

Armed by Asp? C-Terminal Carboxylate in a Dap-Branched Peptide and Consequences in the Binding of Cu^{II} and Electrocatalytic Water Oxidation

by

Ł. Szyrwiel*[,a], D. Lukács[b], D. F. Srankó[b], Z. Kerner[b], A. Kotynia[c], J. Brasun[c], B. Setner[d], Z. Szewczuk[d], K. Malec[a], J. S. Pap*[,b]

Contents:

---

[a] *Dept. of Chemistry of Drugs, Wrocław Medical Univ., ul. Borowska 211, 50-552 Wrocław, Poland. E-mail:*l.szyrwiel@gmail.com.
[b] *Surface Chemistry and Catalysis Dept., MTA Centre for Energy Research, H-1121 Budapest, Konkoly Thege str. 29-33, Hungary. E-mail:pap.jozsef@energia.mta.hu.*
[c] *Department of Inorganic Chemistry, Wrocław Medical University, ul. Borowska 211a, 50-552 Wroclaw, Poland.*
[d] *Faculty of Chemistry, Univ. of Wrocław, ul. F. Joliot-Curie 14, 50–383 Wrocław, Poland.*

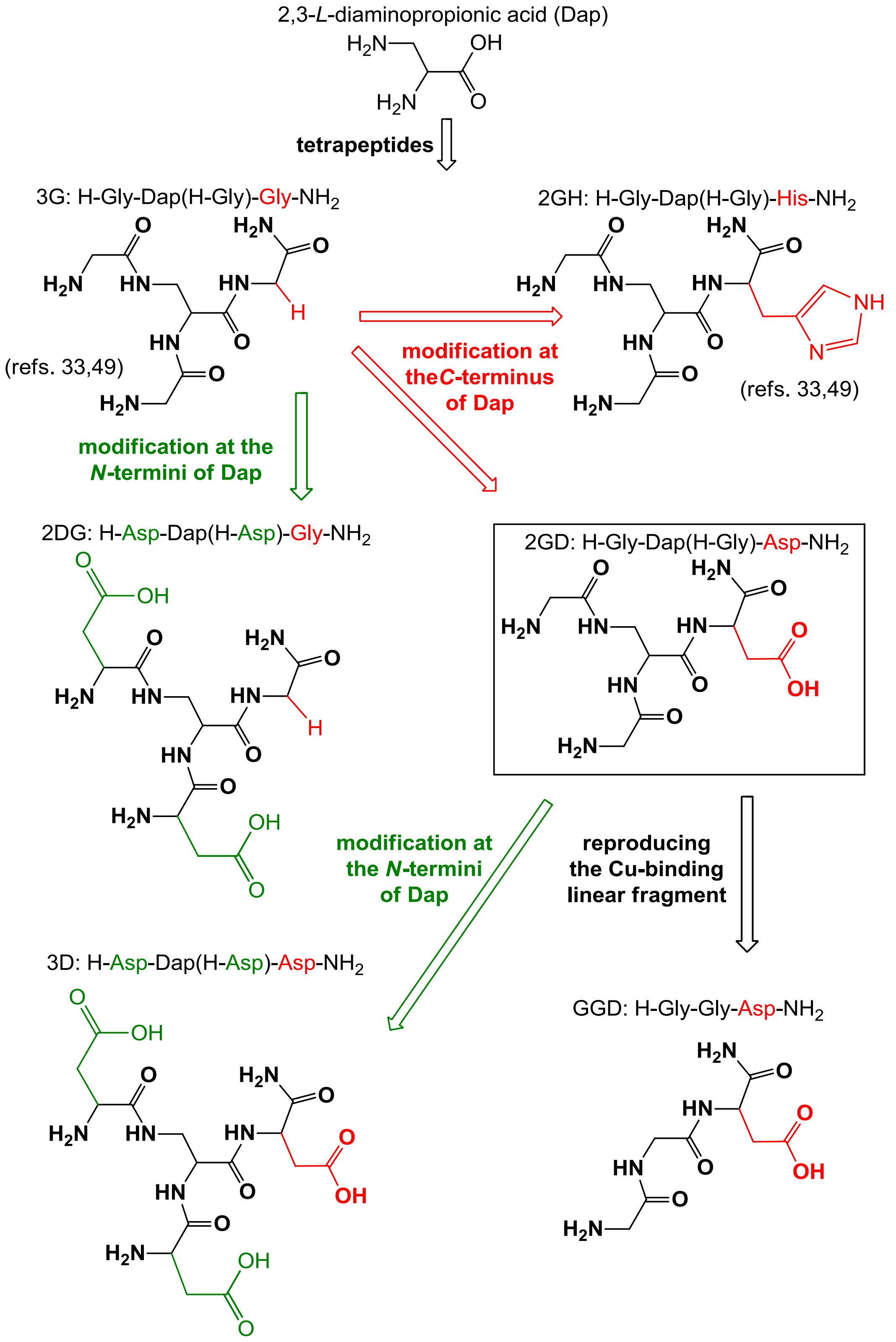

Scheme S1. Ligands discussed in this study and their relation to 2GD (the effect of the different substitutions on the water oxidation activity is discussed in the text).

Table S1. X-Band EPR parameters from simulation for the **Cu-2GD** equilibrium macro-species.[a]

	Cu$_2$(2GD)$_2$H$_{-3}$ and Cu(2GD)H$_{-2}$[b]	Cu(2GD)H$_{-3}$
$g_{//}$ (g_z)	2.2070	2.2014
$g_{\perp}$ (g_x, g_y)	2.0441, 2.0530	2.0421, 2.0528
$A^{Cu}_{//}$ (A^{Cu}_z)	196	196
$A^{Cu}_{\perp}$ (A^{Cu}_x, A^{Cu}_y)	14, 27	16, 27
$a^N_{//}$[c]	10 (3N)	10 (3N)
$a^N_{\perp}$(a_x^N, a_y^N)	13, 15 (3N)	13, 15 (3N)

[a] [$|A|$] = 10^{-4}cm^{-1}, the simulated component spectra for the contributing species were fitted by optimization of the typical couplings of the unpaired electron to the ^{63}Cu and ^{65}Cu nuclei (I = 3/2). Rhombic anisotropy, *e.g.*, splitting of $g_{//}$ to g_x and g_y, at a varying level occurs, indicating distortion in the equatorial ligand geometry.
[b] Cu$_2$(2GD)$_2$H$_{-3}$ and Cu(2GD)H$_{-2}$ were considered with the same parameters
[c] estimation from unresolved structures (the effect is comparable to line broadening)

Table S2. E_{net} values for the Cu$^{III/II}$ redox transition as determined by SWV for **Cu-2GD** and plotted against pH in Fig. 5.

pH	$E°'$(Cu$^{III/II}_{dimer}$) *vs.* Ag/AgCl (V)[a,b]	$E°'$(Cu$^{III/II}$) *vs.* Ag/AgCl (V)[a,b]
7.10	0.802(2)	
7.42	0.801(3)	
7.64	0.802(3)	
7.94	0.802(3)	0.715[c]
8.17	0.803(4)	0.714[c]
8.36	0.804(5)	0.716[c]
8.54	0.804(4)	0.717(4)
8.74		0.715(5)
8.95		0.715(5)
9.16		0.713(4)
9.35		0.712(4)
9.55		0.708(4)
9.80		0.704(3)
10.05		0.704(3)
10.30		0.698(3)
10.58		0.691(3)
10.83		0.680(3)
11.15		0.671(3)
11.44		0.659(3)

[a] error in last digit is indicated in parenthesis
[b] to obtain values against SHE 0.2 V is added to the measured values against the Ag/AgCl ref. electrode
[c] estimated values, not used in calculations

Fitting of the SWV data

The pH-dependence of the E_{net} values (Table S1) associated with the $Cu^{III/II}$ transition of $Cu^{II}(2GD)H_{-2}$ is plotted in Fig. 5. On the analogy to our earlier studies (see refs. 33, 52,56 in the main text) the data points were fitted by arbitrarily appointing a redox equilibrium process shown in eq. (1) and applying it to modify the Nernst equation, eq. (2) in order to explain the pH-dependence of E_{net}. (P. Wardman, *J. Phys. Chem. Ref. Data*, 1989, 1637–1755.) In this equation we presumed that the reduced (Cu^{II}) form participates in one proton dissociation equilibrium, while the oxidized (Cu^{III}) form is involved in two such processes:

$$\mathrm{Cu^{III}(2GD)H_{-3} + H^{+} + e^{-} \rightleftharpoons Cu^{II}(2GD)H_{-2}} \quad (1)$$

$$E_{net} = E°'(\mathrm{Cu^{III}(2GD)H_{-3},H^{+}/Cu^{II}(2GD)H_{-2}}, \mathrm{pH} = 0) + \\ + 0.0591\log \frac{K_{a(red)} + [\mathrm{H^{+}}]}{1 + \dfrac{[\mathrm{H^{+}}]}{K_{a(ox1)}} + \dfrac{K_{a(ox2)}}{[\mathrm{H^{+}}]}} \quad (2)$$

, where $K_{a(red)}$ is the acid dissociation constant of $Cu^{II}(2GD)H_{-2}$ to $Cu^{II}(2GD)H_{-3}$, $K_{a(ox1)}$ and $K_{a(ox2)}$ are the acid dissociation constants for the $Cu^{III}(2GD)H_{-2}$ to $Cu^{III}(2GD)H_{-3}$ and the $Cu^{III}(2GD)H_{-3}$ to $Cu^{III}(2GD)H_{-4}$, respectively, $E°'$ ($Cu^{III}(2GD)H_{-3},H^{+}/Cu^{II}(2GD)H_{-2}$, pH = 0) is the formal potential of the process in eq. (1). The number of pK_a parameters was based on the consideration of a deprotonation step confirmed for $Cu^{II}(2GD)H_{-2}$ by potentiometry ($pK_{a(red)} = 10.56$). Regarding the *E vs.* pH data pattern in Fig. 5b this $pK_{a(red)}$ has to be accompanied by two deprotonations for the oxidized complex forms (in principle the data could be fitted with only one $pK_{a(ox)}$ giving similar $E°'(Cu^{III}(2GD)H_{-2}/Cu^{II}(2GD)H_{-2})$, however, only by worse fitting and ignoring the existence of $pK_{a(red)}$). Note that UV-vis, EPR and CD spectroscopic changes also indicate a slight increase in the ligand field strength in this pH region in line with the existence of a deprotonation step for the Cu^{II} complex.

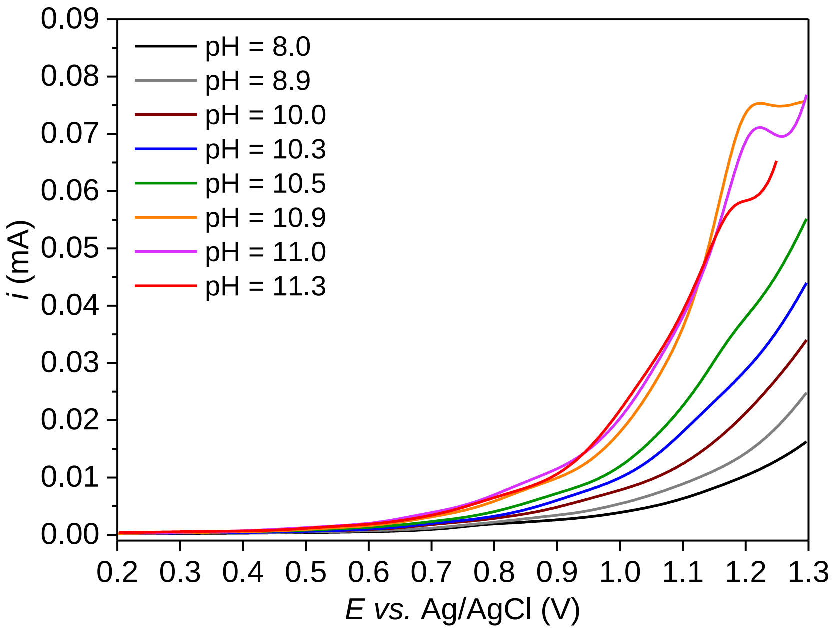

Figure S1. Dependence of the linear sweep voltammetry response on the pH (scanned to the anodic direction, [**Cu-2GD**] = 0.38 mM, $\nu = 25$ mVs^{-1}, in 0.15 M phosphate electrolyte at 25°C, GC working electrode, corrected with the buffer-only currents at each pH).

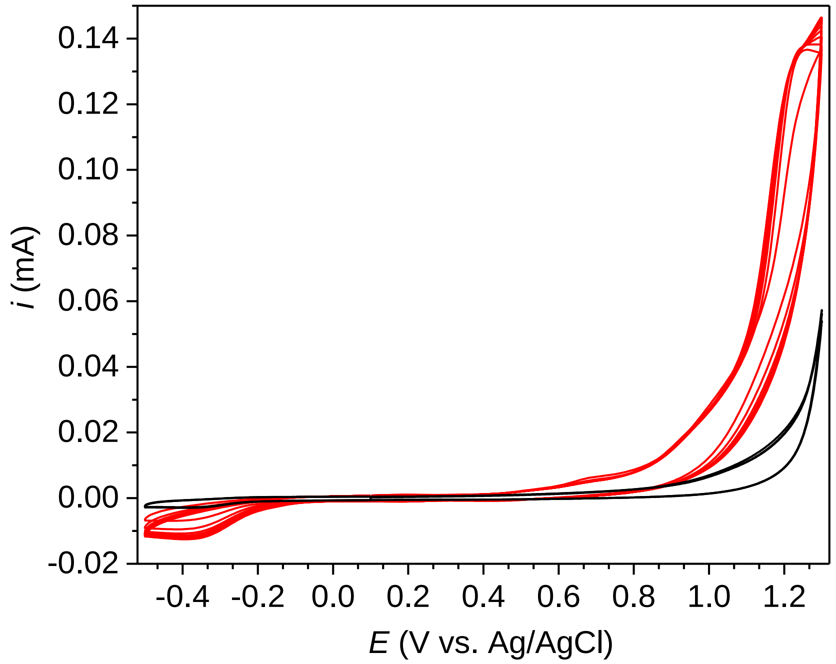

Figure S2. Red curve: CV (10 cycles) of a [**Cu-2GD**] = 0.76 mM solution (see also Fig. S9), $\nu = 25$ mVs^{-1}, pH = 11.02, in 0.2 M phosphate at 25°C. Working electrode: 0.071 cm^2 glassy carbon. Black curve: CV recorded on the same electrode in phosphate only, after rinse, under Ar.

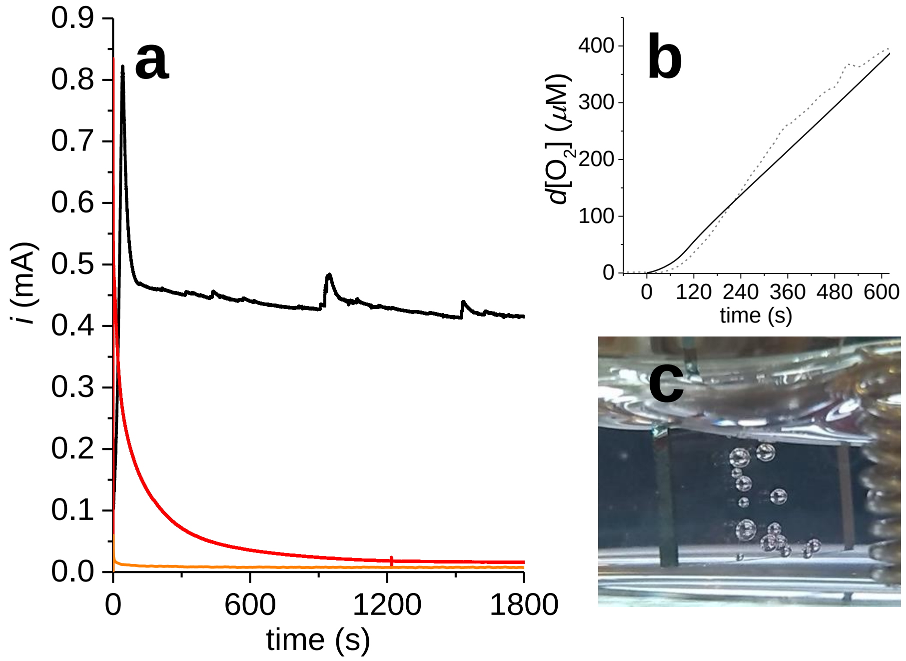

Figure S3. a) Controlled potential electrolysis (CPE) at 1.2 V *vs.* Ag/AgCl with a 0.57 mM solution of **Cu-2GD**, in 0.2 M phosphate (pH = 11), at 25°C, by using an ITO working electrode (~0.8 cm^2), no stirring applied – black curve: CPE of the **Cu-2GD** solution; red curve – CPE with the used ITO electrode in a new phosphate solution under identical conditions; orange curve – CPE current on an unused ITO in the same solution; b) initial O_2 production measured with a fluorescence probe in a stirred solution near the working electrode in a sealed 4 mL cell (dotted line, $t = 0$ indicates the start of CPE, before that the O_2 concentration was steady), the change in O_2 concentration was also calculated from the measured charge (Q, solid line) during CPE at 1.2 V *vs.* Ag/AgCl, fitted with a 90% Faradaic efficiency (*i.e.*, $d[O_2]$ (μM) = $10^9 Q/(0.9nFV)$, where Q = [C], n = 4, F = 96485 C/mol, V = 4 mL) and compared to the detected; c) bubble formation on the surface of ITO in a non-stirred experiment (the small peaks in the current in a) are caused by the spontaneous breakaway of gas bubbles).

Table S3. XPS surface composition of ITO after 0.5 and 6.0 hour CPE at 1.2 V *vs.* Ag/AgCl with a 0.57 mM solution of **Cu-2GD**, in 0.2 M phosphate (pH = 11), at 25°C, (A_{ITO}~0.8 cm^2).

elements / component peak	Binding energy (eV)		Chemical states	Surface conc. (at.%)	
	0.5 h	6.0 h		0.5 h	6.0 h
Cu 2p	933.0	933.0	Cu(I)	0.3	0.7
O 1s	530.1	529.9	Oxides	33.3	25.0
	531.1	530.7	Oxides, hydroxides, PO_4^{3-}	7.8	8.3
	532.0	531.6	O=C	16.0	19.0
	533.5	533.0	O–C	1.8	3.4
Sn 3d	486.7	486.7	SnO, SnO_2	2.7	2.6
In 3d	444.6	444.7	In_2O_3	19.6	19.5
N 1s	399.1	399.8	peptide, amine	0.8	1.7
C 1s	284.8	284.8	C–C, C–H	12.3	14.5
	286.4	286.3	C–O, C–N, C=N	3.6	3.6
	288.4	288.6	C=O	0.8	1.4
	289.4	290.6	O–C=O, π–π* satellite	0.7	0.3
P 2p	133.2	133.2	PO_4^{3-}	0.3	0.2

X-ray photoelectron spectroscopy (XPS) on ITO after CPE in a solution of Cu-2GD

The binding energy of the *Sn 3d* and *In 3d* peaks were assigned to their oxides (*Sn* $3d_{5/2}$ = 486.7 eV and *In* $3d_{5/2}$ = 444.6 eV) and the use of the ITO surface in electrochemistry did not cause any changes in their chemical states. *Note that the relative percentage of the elements (Cu, N, P) that can be unambiguously attributed to a deposited fraction of components from bulk solution is too low to draw any quantitative conclusions and the following discussion rather serves as qualitative evidence for the presence of peptides, Cu^{II} bound in complex and carboxylate groups on the surface.*

The copper content was determined either after 0.5 hour of chronoamperometric treatment at 1.2 V *vs.* Ag/AgCl both by the presence of *Cu 2p* (Fig. S4) and by the *Cu LMM* peaks. The *Cu* $2p_{5/2}$ peak is observed at 933.0 eV while the position of the *Cu* $2p_{3/2}$ is at ~952.7 eV. These are typical for the Cu^{I} state,[S1] however, Cu^{II} compounds are known to be sensitive of the reductive environment of ultra-high vacuum conditions. The modified Auger parameter, α' = 1846.8 eV value (ref. 48 of the main text) is typical for the copper in organic environment bound to nitrogen,[S2] and thus confirms the presence of Cu bound by nitrogen donor groups.[S3]

There is considerable carbon content on the surface. The peak at 284.8 eV is related to C-C/C-H bonds (Fig. S4). The peak at 286.4 eV is typical for carbon in C-O as well as for C-N and C=N bonds,[S4-S6] whereas the 288.4 eV peak can be assigned to the carbon in C=O bonds of amide groups.[S4-S6] The peak at ~290 eV can indicate the presence of some O-C=O groups or it can be assigned to π–π* satellite.

The majority of the oxygen content originates from inorganic compounds such as oxides, hydroxides or phosphates (Fig. S4). The oxides and hydroxides are components of the ITO substrate, while phosphate is built into the film from the buffer solution. Supporting, a peak appears at 133.2 eV characteristic for $P\ 2p_{3/2}$ in phosphate. This value corroborates the presence of phosphate and clearly attributes some of the oxygen at 530.7 eV to the phosphate.[S7] The *O 1s* peaks appearing at higher binding energies can be assigned to the oxygen in organic compounds. The *O 1s* at 531.6 eV is a characteristic for the O=C bond and the 533.0 eV signal is ascribed to O–C bonds.[S7]

Nitrogen content was detected at peak energies that are typical for an organic environment (Fig. S4). The peaks at 399.1 eV and 399.8eV are assigned to the *N 1s* in amide or in amine chemical state. Altogether these results indicate that there is a stable Cu-complex film formed on the surface.

References

(S1) Truica-Marasescu, F.; Wertheimer, M. R. *Plasma Proc. Polym.* **2008**, *5*, 44-57.

(S2) Briggs, D.; Brewis, D. M.; Dahm, R. H.; Fletcher, I. W. *Surf. Interface Anal.* **2003**, *35*, 156-167.

(S3) Shard, A. G.; Whittle, J. D.; Beck, A. J.; Brookes, P. N.; Bullett, N. A.; Talib, R. A.; Mistry, A.; Barton, D.; McArthur, S. L. *J. Phys. Chem. B* **2004**, *108*, 12472-12480.

(S4) Wagner, C. D.; Naumkin, A. V.; Kraut-Vass, A.; Allison, J. W.; Powell, C. J.; Rumble Jr., J. R. *NIST Standard Reference Database 20*, Version 3.4 (web version) (http:/srdata.nist.gov/xps/) **2003**.

(S5) Gaarenstroom, S. W.; Winograd, N. *J. Chem. Phys.* **1977**, *67*, 3500-3506.

(S6) Arkhipushkin, I. A.; Yu. E. Pronin, Vesely, S. S.; Kazansky, L. P. *Int. J. Corros. Scale Inhib.* **2014**, *3*, 78–88.

(S7) S. R. Puniredd, D. Janczewski, D. P. Go, X. Zhu, S. Guo, S. L. M. Teo, S. S. C. Lee, G. J. Vancso, *Chem. Sci.* 2015, **6**, 372.

(S8) Moulder, J. F.; Stickle, W. F.; Sobol, P. E.; Bomben, K. D. *Handbook of X-ray Photoelectron Spectroscopy*, Perkin-Elmer Corp., Eden Prairie, MN, **1992**.

(S9) Beamson, G.; Briggs, D. *High Resolution XPS of Organic Polymers - The Scienta ESCA300 Database*, Wiley Interscience, **1992**.

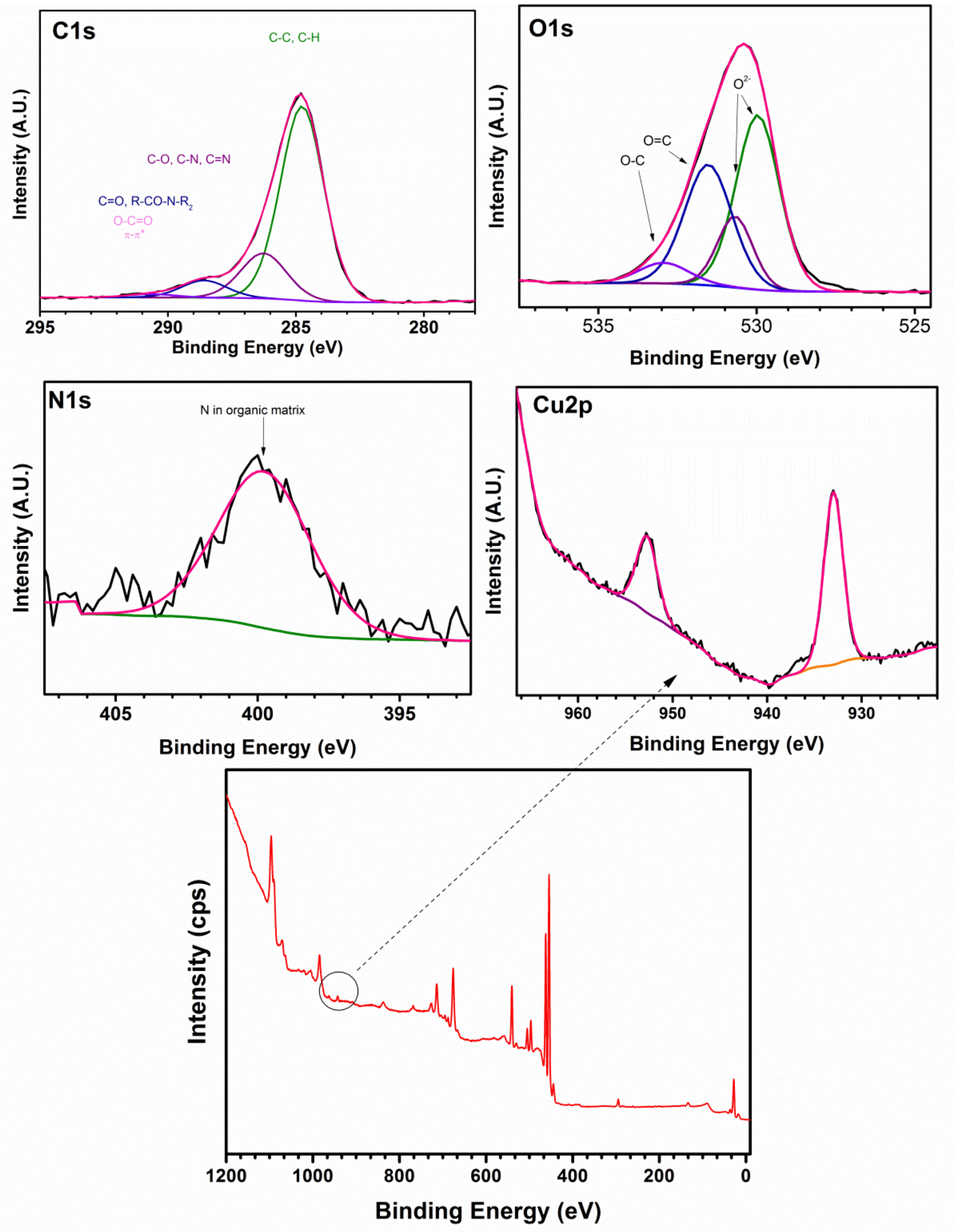
C1s
C-C, C-H
C-O, C-N, C=N
C=O, R-CO-N-R2
O-C=O
π-π*
Intensity (A.U.)
295
290
285
280
Binding Energy (eV)
O1s
O2-
O=C
O-C
Intensity (A.U.)
535
530
525
Binding Energy (eV)
N1s
N in organic matrix
Intensity (A.U.)
405
400
395
Binding Energy (eV)
Cu2p
Intensity (A.U.)
960
950
940
930
Binding Energy (eV)
Intensity (cps)
1200
1000
800
600
400
200
0
Binding Energy (eV)

a

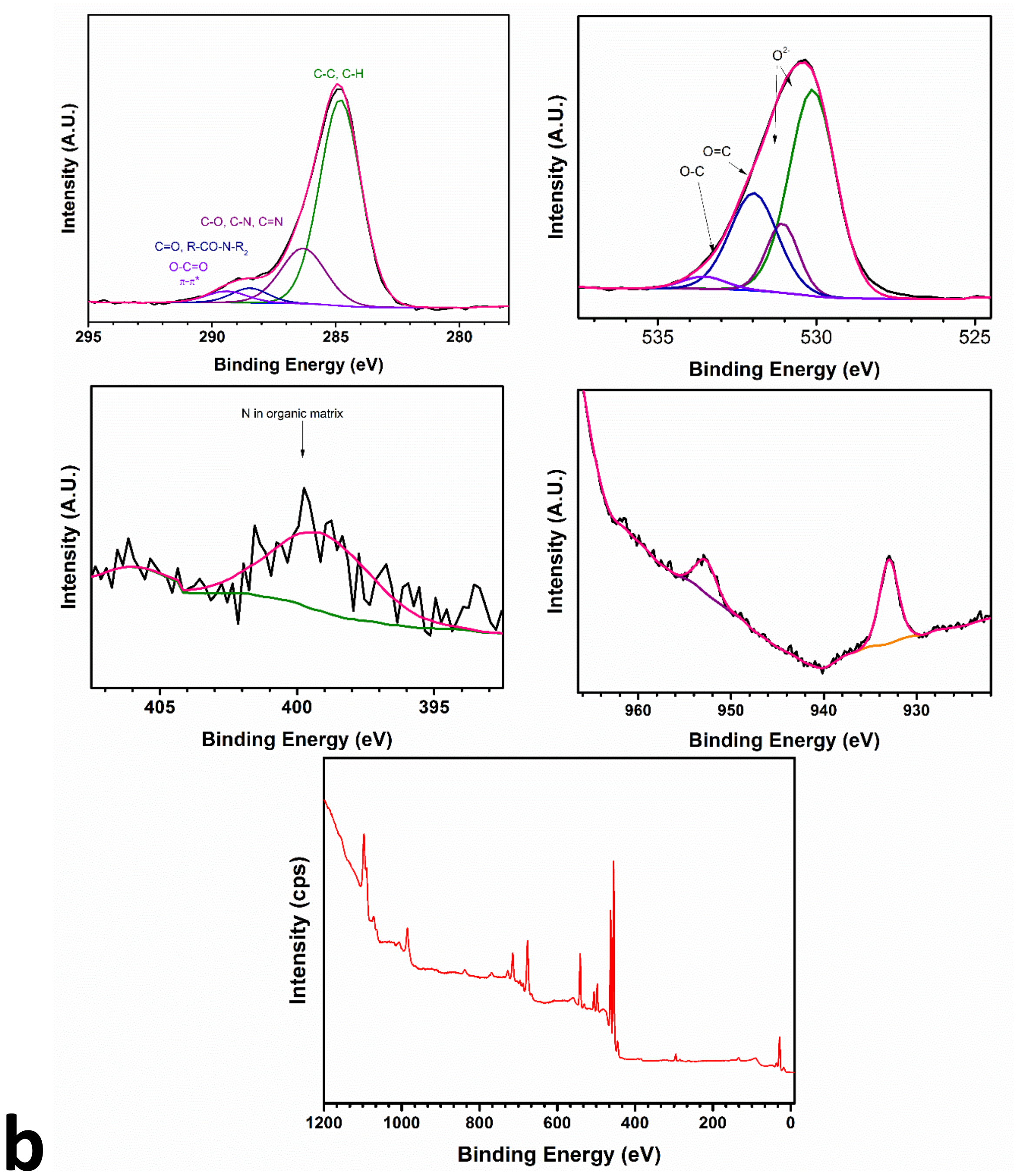

Figure S4. Recorded and fitted XP spectra of the C 1s, O 1s, N 1s and the Cu 2p binding energy regions and the full recorded spectrum, measured on the used ITO working electrode surface after a) 6h, b) 0.5h of CPE at 1.2 V *vs.* Ag/AgCl with a 0.57 mM solution of **Cu-2GD**, in 0.2 M phosphate (pH = 11), at 25°C, (A_{ITO}~0.8 cm^2) .

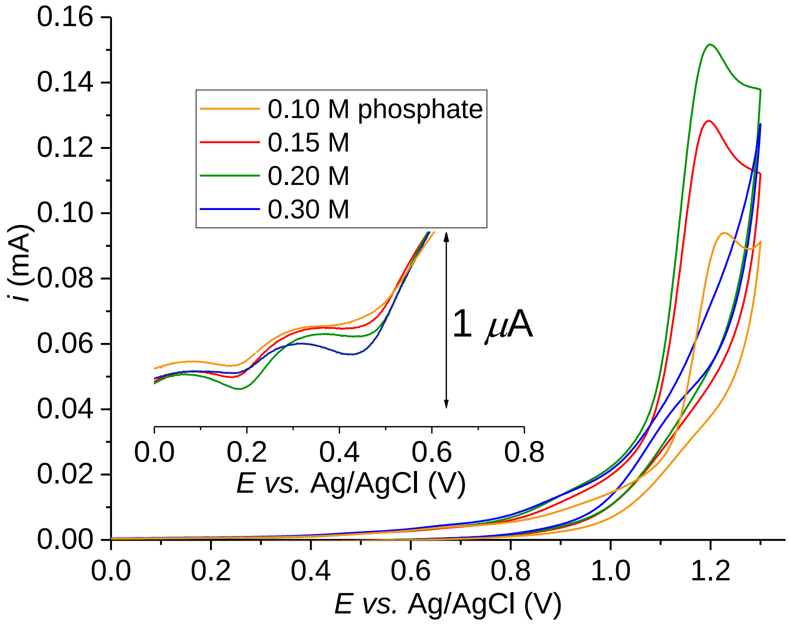

Figure S5. Dependence of the current on the concentration of phosphate, recorded by CV, [**Cu-2GD**] = 0.67 mM, ν = 25 mVs^{-1}, at 25°C, GC working electrode). Inset: blown-up view of the Cu$^{III/II}$ transitions relevant to the mechanistic considerations as detailed in the main text.

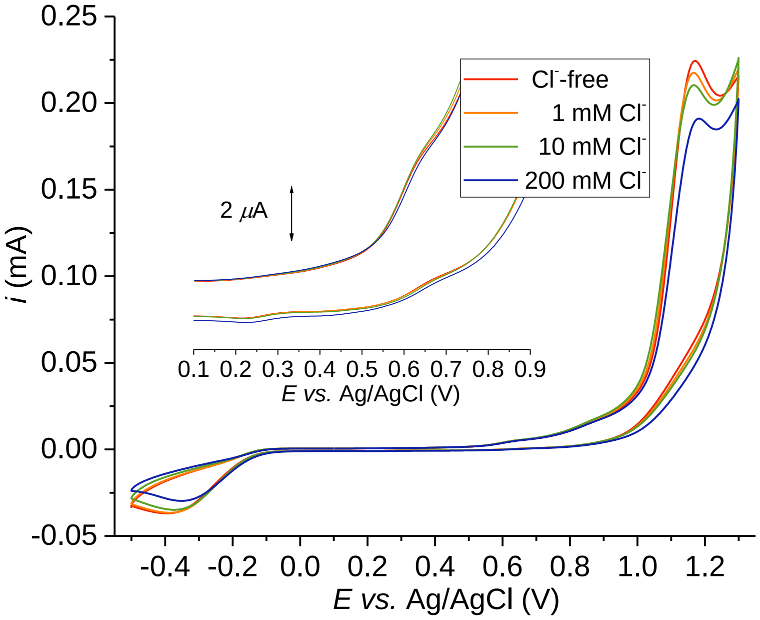

Figure S6. Effect of added chloride to the solution of **Cu-3G** (0.57 mM, 0.2 M PB, pH = 11, 25 mVs^{-1}, GC working electrode). Inset: blown-up view of the plot, where Cu$^{III/II}$ transitions are detected.

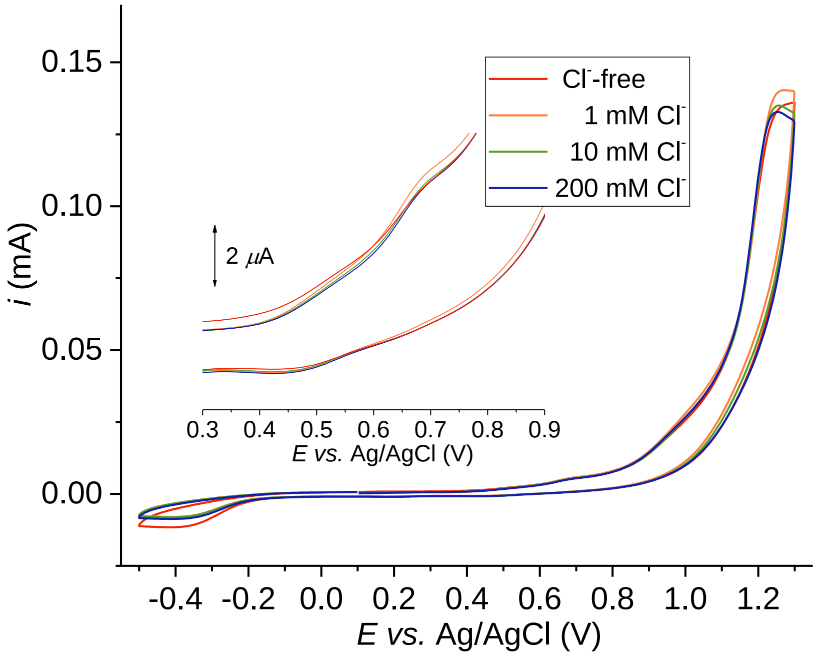

Figure S7. Effect of added chloride to the solution of **Cu-2GD** (0.57 mM, 0.2 M PB, pH = 11, 25 mVs^{-1}, GC working electrode). Inset: blown-up view of the plot, where Cu$^{III/II}$ transitions are detected.

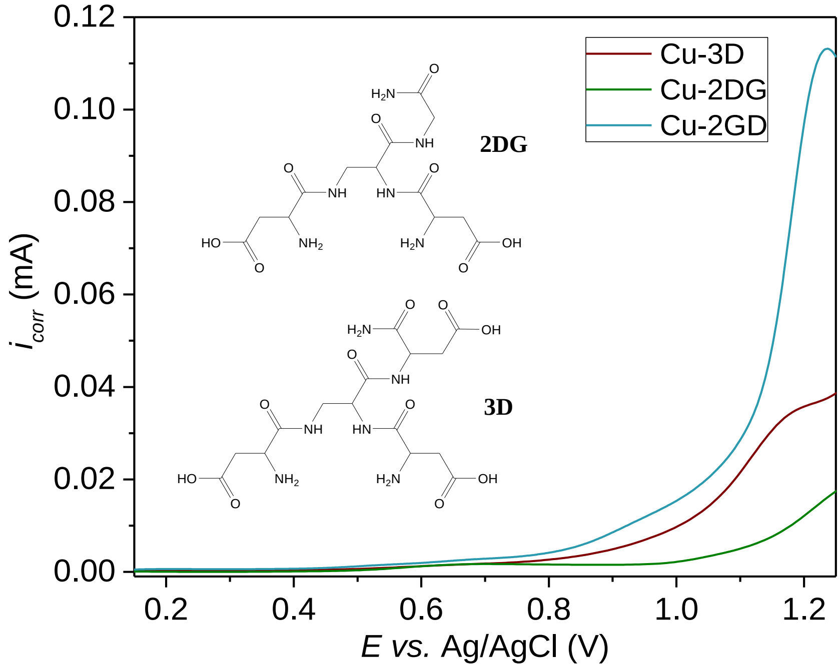

Figure S8. CV curves for Cu : L (0.9:1) systems (L = 2DG or 3D, 0.57 mM, 0.2 M PB, pH = 11, 25 mVs^{-1}, GC working electrode).

Experiments with multi-Asp Dap-branched ligands

Ligand analogs to 2GD with multiple Asp substitutions, namely H-Asp-Dap(H-Asp)-**Gly**-NH_2 (2DG) and H-Asp-Dap(H-Asp)-**Asp**-NH_2 (3D) are synthetically available, therefore we applied them in a similar manner to 2GD to explore the effect of extra N-terminal carboxylates on catalysis. The performance of a Cu^{III} complex can be expected to depend on ligand extensions, which may block the axial sites. Indeed, additional Asp residues in the two available N-terminal these positions almost completely cease catalysis. Since the N-terminal Asp carboxylate groups can hinder the axial coordination sites from external ligands like H_2O or phosphate anion, we presume that this is the reason of the catalytic inactivity of the **Cu-2DG** and **Cu-3D** complexes.

2DG and 3D peptide synthesis

The synthesis of the peptides H-Asp-Dap(H-Asp)-Asp-NH_2 and H-Asp-Dap(H-Asp)-Gly-NH_2 were performed manually on the Rink Amide MBHA resin (loading: 0.52 mM/g) in a polypropylene syringe reactor (Intavis AG, Köln, Germany) equipped with polyethylene filter, according to the standard Fmoc (9-fluorenylmethoxycarbonyl) solid phase synthesis procedure using similar procedure to one published by us previously (see ref. 49 of the main text). TBTU (*O*-(Benzotriazol-1-yl)-*N*,*N*,*N*',*N*'-tetramethyluronium tetrafluoroborate) was used as a coupling reagent (3 equivalents). Oxyma Pure (Ethyl 2-cyano-2-(hydroxyimino)acetate) (3 equivalents) and DIPEA (*N*,*N*-Diisopropylethylamine) (3 equivalents) were used as an additives. DMF (*N*,*N*-Dimethylformamide) was used as a solvent. Each coupling step was performed for 2h. The end of each coupling reaction was confirmed by Kaiser Test. After removal of the Fmoc- protecting groups from the diaminopropionic acid derivative with 25% piperidine in DMF a mixture of Fmoc-His(Boc)-OH/TBTU/Oxyma Pure/DIPEA (6 equivalents of each reagent) in DMF was added and stir for 24h. The end of a coupling was confirmed by Kaiser Test. Peptides were cleaved from the resin simultaneously with the side chain deprotection using a solution of TFA/H_2O/TIS (95/2.5/2.5, v/v/v) at room temperature for 2h, precipitated in cold diethyl ether and purified by the semi-preparative RP-HPLC. Each peptide was purified on a Varian ProStar (Palo Alto, CA, California) with UV detection (210 nm) on a TSKgel ODS-120T 12TG08eh004 column (215 x 30.0 mm, 10 μm) equipped with a TSKguard column ODS (21.5x7.5 mm, 10 μm), with a gradient elution of 0-80% B in A (A = 0.1% TFA in water; B = 0.1% TFA in acetonitrile/H_2O, 4:1) for 40 min (flow rate 7 mL/min). The main peak, corresponding to the peptide, was collected and the fraction was lyophilized. The purified ligands were obtained as it trifluoroacetate salt. Their molecular weights were confirmed by ESI-MS using high-resolution mass spectrometer, Bruker micrOTOF-Q (Bruker Daltonics, Bremen, Germany). The *m/z* obtained for $[M+H]^+$ ions of H-Asp-Dap(H-Asp)-Asp-NH_2 and H-Asp-Dap(H-Asp)-Gly-NH_2 were 449.1653 (calculated 449.1649) and 391.1592 (calculated 391.1591), respectively.

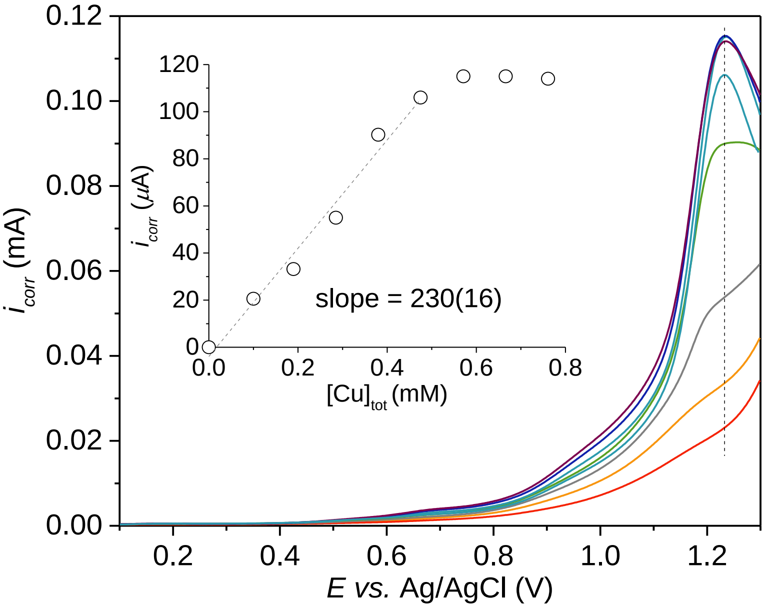

Figure S9. Effect of the concentration of **Cu-2GD** on the catalytic current (scans to the anodic direction were potted corrected with the buffer-only currents, ν = 25 mVs^{-1}, in 0.2 M phosphate electrolyte at 25°C, GC working electrode). The TOF (s^{-1}) value was calculated from the slope by applying equation: i_{cat} (μA) = $n_{cat}FA[\mathrm{Cu}](k_{cat}D_{Cu})^{0.5}$, where n_{cat} = 4, F is the Faraday constant, A = 0.071 cm^2, [Cu]$_{tot}$ is the bulk concentration of **Cu-2GD** (mM), and D_{Cu} is the diffusion coefficient of the complex in 0.2 M PB at pH 11, that is 4.5×10^{-6} cm^{2}s^{-1}.

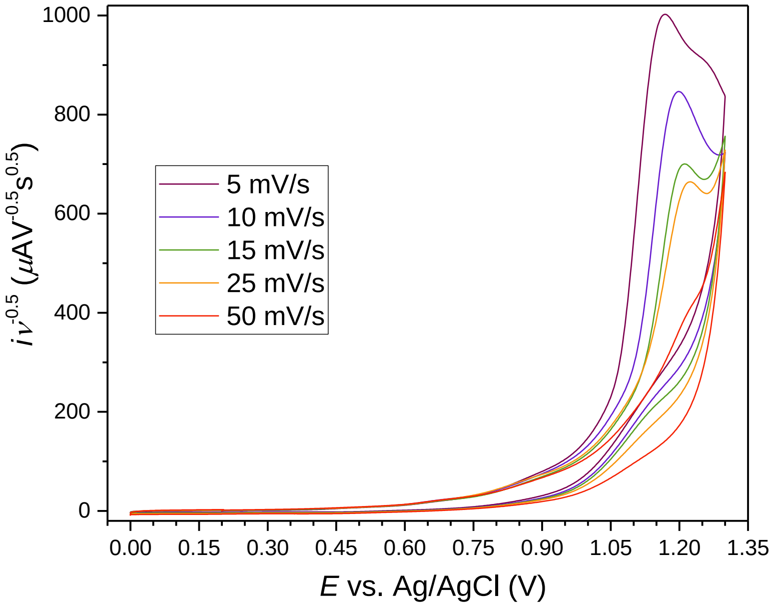

Figure S10. Catalytic current responses with **Cu-2GD** normalized with $\nu^{-0.5}$ (0.47 mM, in 0.2 M phosphate buffer, pH = 11, 25°C on GC working electrode).

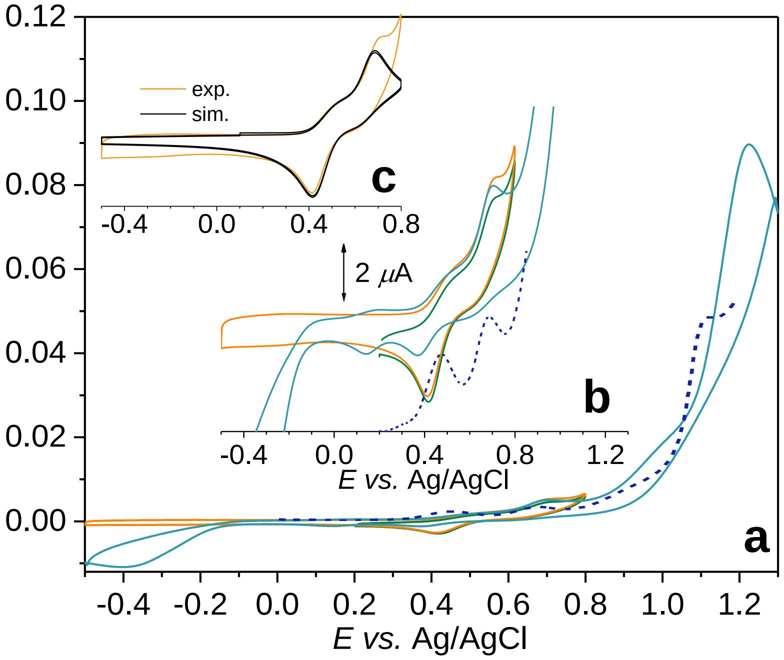

Figure S11. a) CV of **Cu-GGD** at pH = 11, in 0.2 M phosphate electrolyte, c = 0.57 mM, ν = 25 mVs^{-1}, GC working el., started to the anodic direction (reverse points - blue: 1.3/-0.5 V, green: 0.8/0.3 V, orange: 0.8/-0.5 V, black: 0.3/-0.5 V); b) blown-up view of the same CV scans; c) simulation of the Cu$^{III/II}$ current peaks (for simulation parameters see Scheme S4). Dashed blue lines - SWVs of the same samples. Further calculated data on this system: D_{Cu} = 7.5×10^{-6} cm^{2}s^{-1} and k_{cat} ~10 s^{-1}.

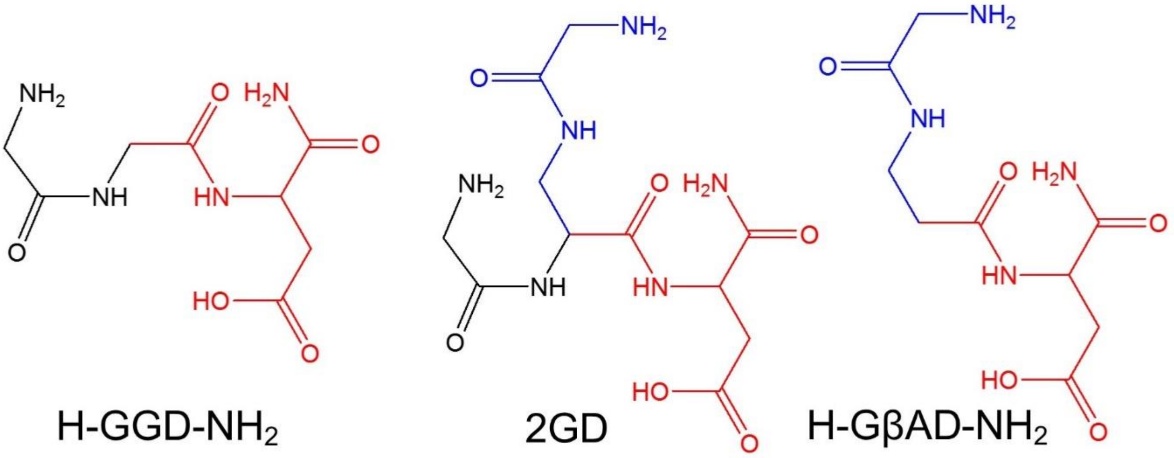

Scheme S2. The structure of the Dap-branched peptide 2GD and its linear domains. Colours correspond to structural fragments that are also included in H-GGD-NH$_2$ or H-GβAD-NH$_2$.

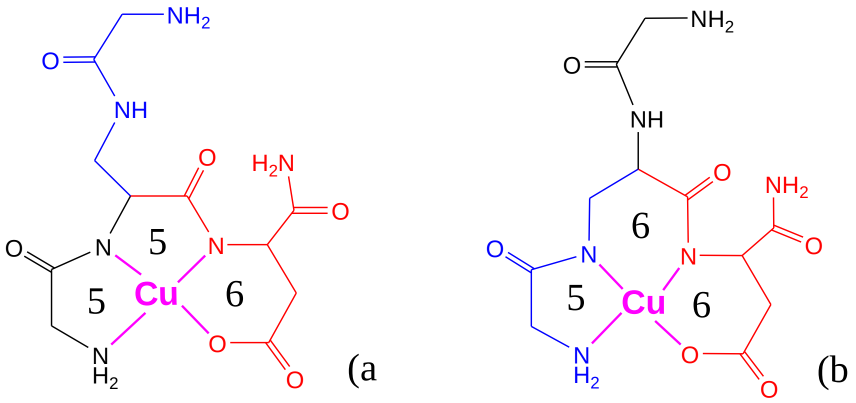

Scheme S3. Two possible isomers of CuLH$_{-2}$ complex species that can be formed in theory with the 2GD ligand. Experimental data support the structural isomer in a). Colours correspond to structural fragments: blue and black to N-terminals and red to C-terminal.

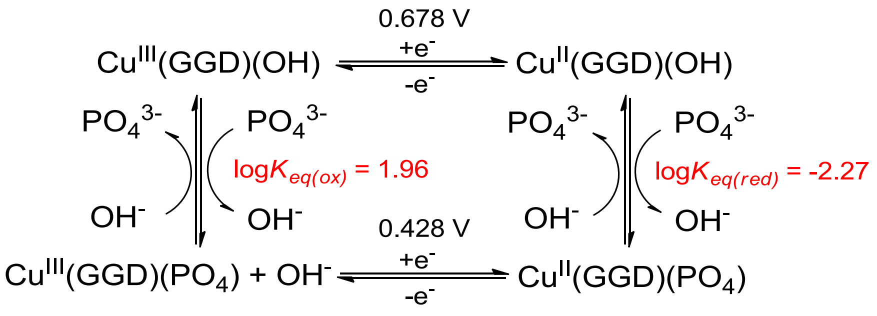

Scheme S4. Equilibrium profile applied for CV simulation in Fig. S11c. Fit parameters - Cu(GGD)(OH): α (transfer coefficient) = 0.5, $k°$ = 8×10^{-3} cms^{-1}; Cu(GGD)(PO$_4$): α = 0.5, $k°$ = 5.3 10^{-3} cms^{-1}; $K_{eq(OX)}$ = k_f/k_b = 500/5.494; $K_{eq(red)}$ = k_f/k_b = 8800/44.6.